Mini-SAOZ Instrument

Ozone and NO_2 column observations
by zenith sky UV-visible spectrometry

Part 1
Scientific Rationale

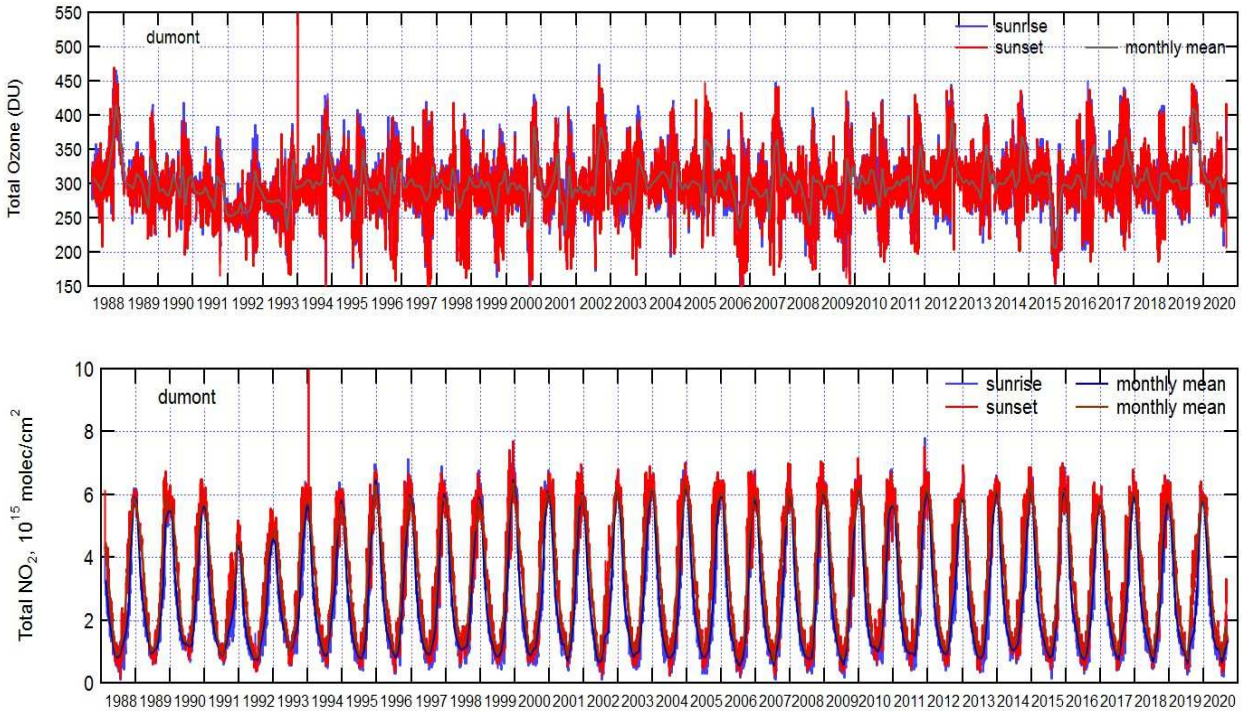

Ozone and NO_2 total column at Dumont, d'Urville, Antarctica, since 1988.

TABLE OF CONTENTS

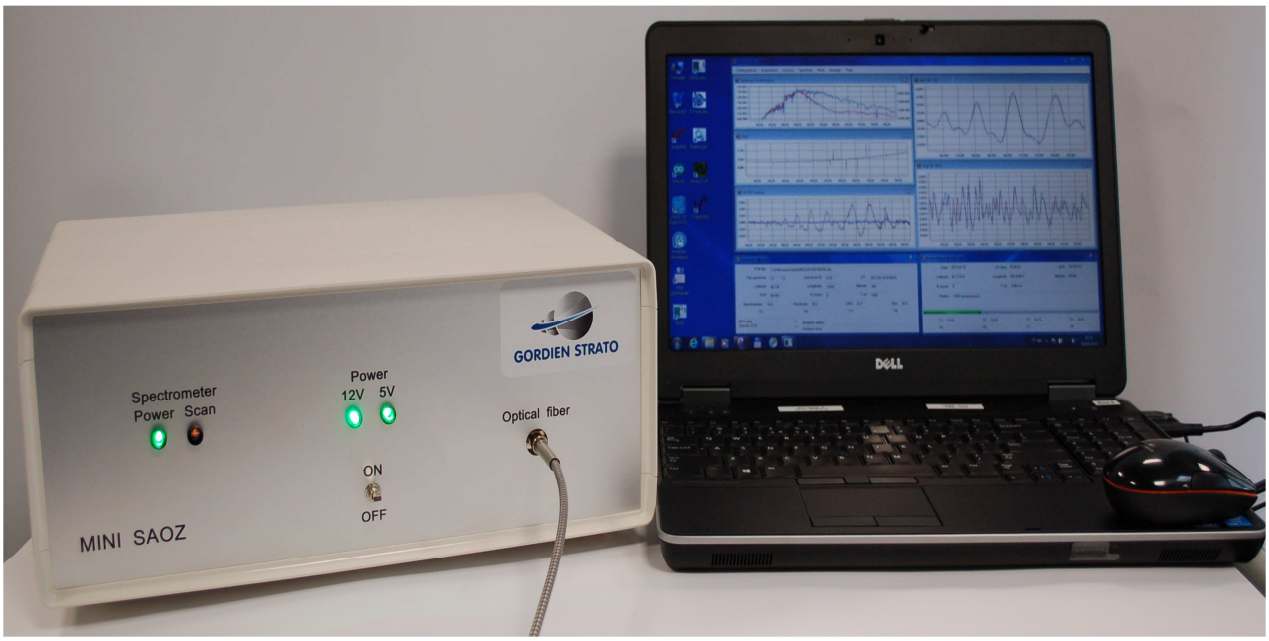

Mini-SAOZ Instrument

Mini-SAOZ box and computer both inside (top), optical fibre with white optical head collecting the zenith skylight and black GPS antenna at the outside (bottom)

GORDIEN STRATO SARL – R.C.S. EVRY 442 128 435
Siège Social/Registered Office : 3, Allée de la Graineterie, 91371 Verrières-le-Buisson, France
Locaux/Offices : Gordien Strato, LATMOS, 11, Boulevard d'Alembert, 78280 Guyancourt, France
gordien.strato@gmail.com ; Tél: + 33 1 80 28 52 52

1. Preface

SAOZ and Mini-SAOZ are UV-Visible spectrometers for monitoring stratospheric ozone (O3) and nitrogen dioxide (NO2). The SAOZ (Système d'Analyse par Observation Zénithale) instrument has been developed in the late eighty's (Pommereau and Goutail, 1988). The Mini-SAOZ is a modernized and lighter version of the SAOZ where all obsolete components have been replaced. The SAOZ is using an holographic flat field spectrometer equipped with a 1024 pixels diode array detector, whereas the Mini-SAOZ is using a Czerny-Turner spectrometer equipped with a flat field grating and a two dimension CDD detector of 2048 x16 pixels. The Mini-SAOZ is designed to work in the inside with a long optical fiber and an optical head at the outside to collect the sunlight.

Ozone is measured in the visible Chappuis bands by comparing the spectra to laboratory cross-sections by the technique of differential optical absorption spectroscopy (DOAS). This method is a relative method, thus not requiring calibration, the measurement being provided by correlation with cross-sections identical for all instruments. The ozone cross sections in the visible range are known to have an uncertainty of 1% with a temperature dependence of less than 1%. Both, SAOZ and Mini-SAOZ instruments are measuring also total NO_2 (mainly stratospheric except in polluted areas where the instrument can provide also the tropospheric NO_2 column) and Polar Stratospheric Clouds (PSCs) thickness or aerosol in case of volcanic eruption.

The precision in ozone slant column measurements at twilight (the solar light scattered at zenith during twilight) is of ~0.5 DU for SAOZ and ~0.3 DU for Mini-SAOZ (less than 0.15 %). The largest error in the vertical total ozone column comes from the Air Mass Factor (AMF) used for converting slant columns into vertical columns. As explained in Hendrick et al. (2011), using the AMF calculated from the TOMS ozone profile climatology results in an uncertainty of 3-4%. The absolute accuracy, resulting from the addition of measurement precision, cross-section and AMF uncertainties, is of the order of 4-5%, similar for both instruments.

The major difference between SAOZ/Mini-SAOZ in the visible Chappuis band and ground-based Brewer/Dobson and satellites instruments, all working in the UV, is coming from the temperature dependence of the ozone cross-sections in the UV. When corrected for this temperature dependence, UV satellites instruments (TOMS, GOME, SCIAMACHY etc…), Brewer and Dobson, agree with SAOZ within less than 2% at mid-latitude and in the tropics, but the difference is larger in polar regions and variable with the satellites (Hendrick et al., 2011).

One of the advantages of SAOZ/Mini-SAOZ compared to other instruments measuring in the UV is the continuous monitoring of total ozone and NO_2 up to 91° Solar Zenith Angle (SZA) that is throughout the whole winter at latitude up to the polar circle, at sunrise and sunset. Another advantage is their capacity to perform measurements in all weather conditions even in the presence of clouds, that is 365 days /year.

The SAOZ/Mini-SAOZ instruments have been deployed all around the world. The current location of the spectrometers is shown in Figure 1.

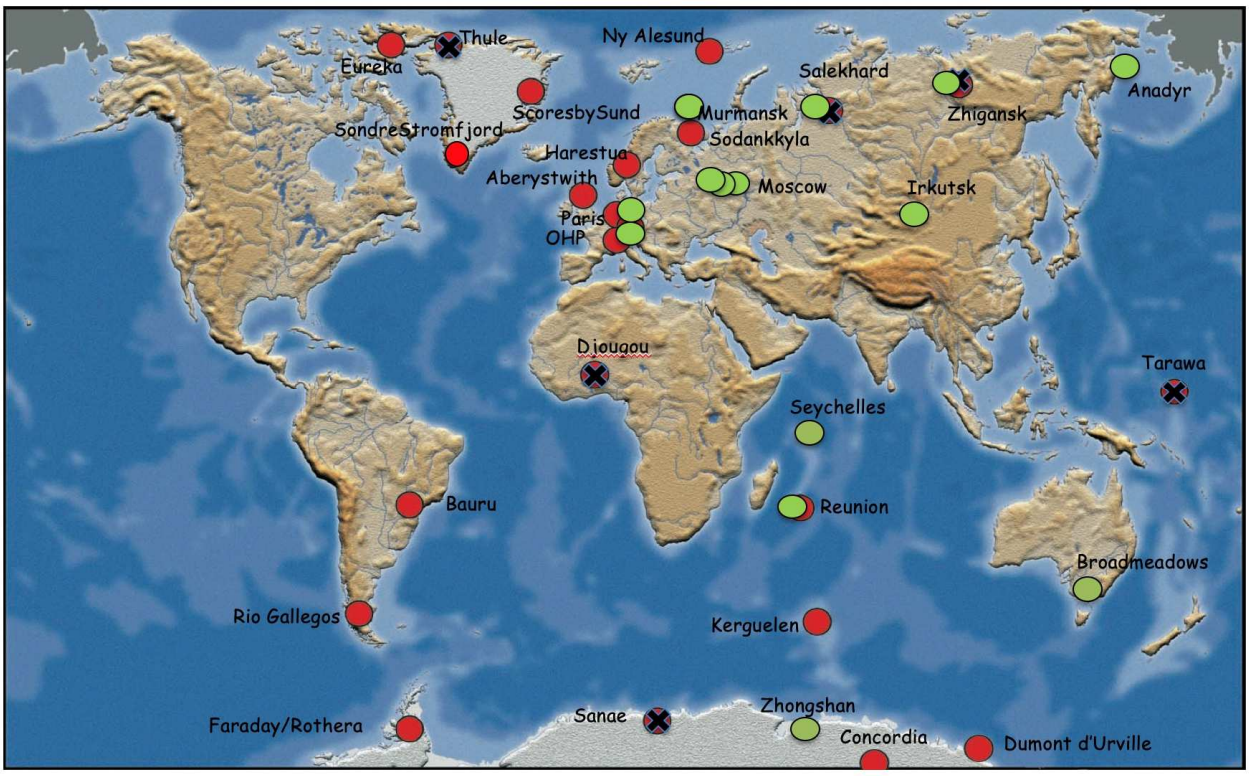

Fig. 1. Deployment of SAOZ (red circles) and Mini-SAOZ (green circles) around the world.

The instruments are fully automatic and the data are available in real time. For the CNRS instruments, ozone and NO_2 columns are displayed in real time on the SAOZ web site: http://saoz.obs.uvsq.fr/SAOZ-RT.html.

The other useful links are:
http://gaw.empa.ch/gawsis/reports.asp?StationID=2076202720
http://gaw.empa.ch/gawsis/reports.asp?StationID=89

SAOZ Scientific Contact:
Dr. Andrea Pazmino
Dr. Manuel Pinharanda
Dr. Florence Goutail
Dr. Jean-Pierre Pommereau
LATMOS
11 Boulevard d'Alembert
78280 Guyancourt, France
andrea.pazmino@latmos.ipsl.fr
manuel.pinharanda@latmos.ipsl.fr
Florence.Goutail@latmos.ipsl.fr
jean-pierre.pommereau@latmos.ipsl.fr

Mini-SAOZ Technical Contact:
Dr. Milena Martic
Managing Director
Gordien Strato at LATMOS
11 Boulevard d'Alembert
78280 Guyancourt
Tel : 33 1 80 28 53 24
Cell : 33 6 71 58 95 56
milena.martic@latmos.ipsl.fr

2. Introduction

2-1 General

The first spectrometer measuring ozone in the stratosphere was the Dobson spectrophotometer invented in 1926. Over one hundred of these spectrometers were deployed in a worldwide network for measuring the total column ozone. They measure the absorption at selected pairs of wavelengths between 300 and 350 nm, whereby ozone absorbs strongly at one wavelength and less at the other. The Dobson spectrometer uses prisms as the dispersive elements. Original versions used photographic plates as the detector. Later ones were modified for a photomultiplier tube.

In 1973, Brewer, McElroy & Kerr used a visible spectrometer to measure NO_2 column amount at its absorption bands between 400 and 450 nm. The spectrometer used a grating as the dispersive element and a photomultiplier as the detector. Many scientists have used the same design principle to measure NO_2 from the ground (Noxon, McKenzie & Johnston) and from balloons (Iwagami, Pommereau & Goutail). In a novel later design, which eliminated errors and backlash in the grating drive, Kerr & McElroy developed a spectrometer with a fixed grating and five exit slits, a rotating mask and a single photomultiplier as detector. Known as Brewer spectrophotometers, some tens of these have been distributed worldwide to make routine measurements of O_3 or NO_2 columns.

Developments of diode-array detectors led to the design of spectrometers with fixed gratings that could measure a continuous spectrum. A design by Schmeltekopf using a Reticon array was deployed in Antarctica for short periods by Mount, Solomon and others in 1986 and 1987 to measure NO_2, NO_3, O_3, OClO and BrO. In 1987, Pommereau and Goutail at CNRS elaborated on this concept using a flat field spectrometer from Jobin-Yvon with an aperture of f/2.9 for high energy throughput and an uncooled diode array Hamamatsu detector of high sensitivity and low dark-current. The spectrometer was combined with a reliable desktop computer and an environmentally sealed case for building the automatic SAOZ UV-Visible instrument. Following the development of diode-array detectors (1024 pixels instead of 512) and computers/software (HP basic replaced by PC Microsoft OS), the first SAOZ 512 HP version has been replaced by the SAOZ 1024 PC version.

The SAOZ instrument is part of the international Network for the Detection of Atmospheric Composition Change (NDACC). The first SAOZ was installed in 1988 and since then deployed at more than 20 stations distributed at all latitudes. SAOZ data are used to report on important scientific subjects such as the ozone layer (Goutail et al. 2005, Kuttipurath et al., 2013, Pommereau et al., 2013) or local NO2 pollution in big cities like Paris, France (Dieudonné et al., 2013).

A miniaturized version of the SAOZ, named Mini-SAOZ, has been recently developed, which will progressively replace “old” SAOZ instrument experiencing aging problems. The Mini-SAOZ is made of a miniaturized Czerny-Turner spectrometer and a 2048 x 16 CCD detector. The light comes through a long optical fibre that allows keeping the spectrometer in the inside while the fibre optics entrance only is exposed at the outside. The instrument is coupled to a laptop PC computer with Microsoft OS.

Newly available Mini-SAOZ developed by LATMOS/ GORDIEN STRATO has been qualified for more than two years of collocated measurements with regular SAOZ at Haute Provence Observatory (OHP) and Guyancourt in France. A prototype of the Mini-SAOZ has also participated in international inter-comparison campaigns in Cabauw, Netherland, in 2009 (Pieters et al., 2012) and 2016 (Kreher et al., 2020).

Long series of SAOZ ozone comparisons with other ground-based (Dobson, Brewer) and satellites (TOMS, SBUV, GOME, GOME-2, SCIAMACHY, OMI) available data, have been reported in Hendrick et al. (2011). Figure 2 shows the long-term comparison between SAOZ/Mini-SAOZ, Dobson, and the data of the various satellites available above OHP in France. Those data are used in all ozone series evaluation projects: ESA CCI (Koukouli et al., 2014), ESA ACVE, EU NORS project, WMO Antarctic ozone bulletins (cf. http://www.wmo.int/pages/prog/arep/gaw/ozone/index.html), NDACC reports and WOUDC daily ozone maps.

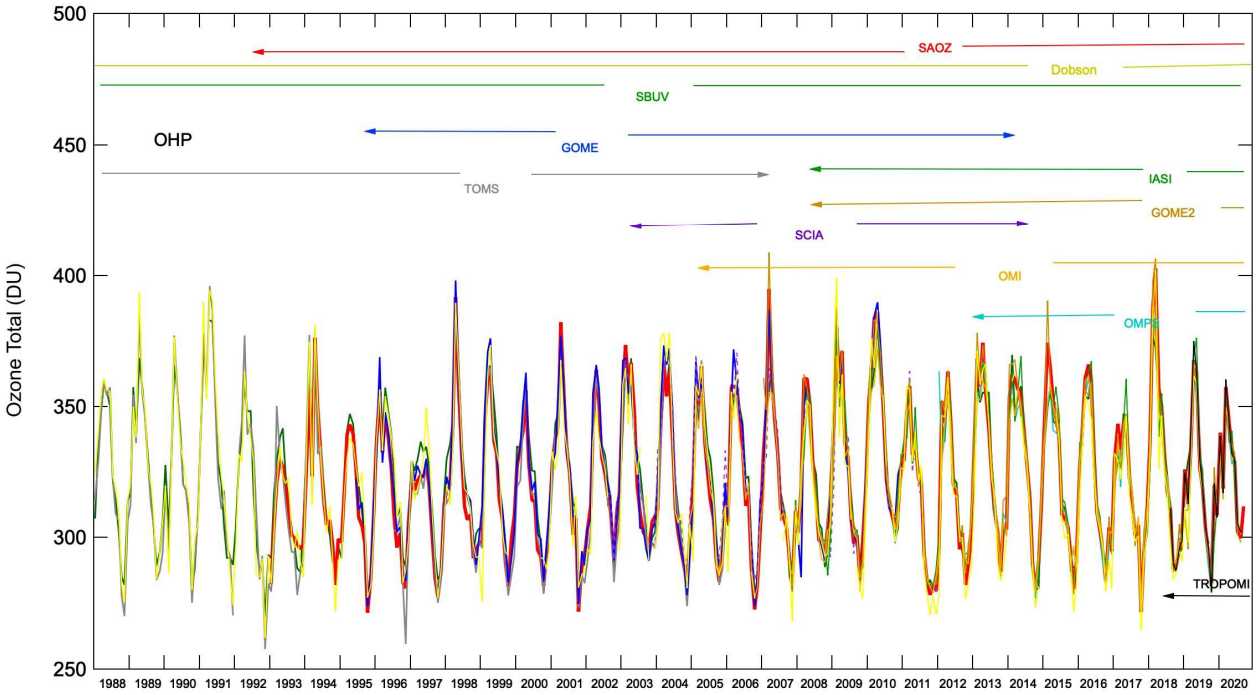

Fig. 2 SAOZ, Mini-SAOZ, Dobson and satellites (SBUV, TOMS, GOME, SCIAMACHY, OMI, GOME 2, OMPS, TROPOMI) long-term comparisons above Observatoire de Haute Provence (OHP) in France.

The SAOZ/Mini-SAOZ instruments have been installed all around the world. For example the Mini-SAOZ has been installed for the first time in late 2010 at the Hydrometeorological Observatory of Anadyr, in the Russian Far East polar region. The first measurements in Anadyr have shown a good agreement with other SAOZ observations at similar latitude and similar stratospheric conditions. Since then the Russian ozone network has been renewed with ten Mini-SAOZ instruments (from Gordien Strato Co. between 2011-2014).

The current list of SAOZ/Mini-SAOZ instruments is shown in Table 1. Other Mini-SAOZ installations are planned or already installed in France, Russia, China, Australia and Seychelles Islands.

Table 1: Location of SAOZ/ Mini-SAOZ spectrometers in 2020, starting date and institutions owning the instrument. All SAOZ instruments are NDACC qualified. Mini-SAOZ are highlighted in grey.

Station	Country	Location	Start/end	Owner	Instrument
Eureka	Canada	80°N, 86°W	2005	CNRS	SAOZ
NY-Alesund	Spitzbergen	79°N, 12°E	1990	NILU	SAOZ
Thule	Greenland	77°N, 69°W	1990/2017	DMI	SAOZ
ScoresbySund	Spitzbergen	70°N, 22°W	1991	CNRS/DMI	SAOZ
Murmansk	Russia	68°N, 33°E	2012	CAO	Mini-SAOZ
Zhigansk	East Siberia	67°N, 123°E	1991/2013	CNRS/CAO	SAOZ
Zhigansk	Russia	67°N, 123°E	2012	CAO	Mini-SAOZ
SondreStromfjord	Greenland	67°N, 51°W	2017	CNRS/DMI	SAOZ
Sodankyla	Finland	67°N, 27°E	1990	CNRS/FMI	SAOZ
Salekhard	West Siberia	67°N, 67°E	1998/2016	CNRS/CAO	SAOZ
Salekhard	West Siberia	67°N, 67°E	2013	CAO	Mini-SAOZ
Anadyr	Russia	65°N, 177°E	2011	CAO	Mini-SAOZ
Dolgoprudny	Russia	56°N, 37°E	2010	CAO	Mini-SAOZ
Irkutsk	Russia	52°N, 104°E	2014	CAO	Mini-SAOZ
Aberystwyth	Wales	52°N, 4°W	1991	U. Manchester	SAOZ
Paris	France	49°N, 2°E	2005	CNRS	SAOZ
Guyancourt	France	49°N, 2°E	2011	CNRS	Mini-SAOZ
Guyancourt	France	49°N, 2°E	2010	CNRS	SAOZ
Jungfraujoch	Switzerland	47°N, 8°E	1990/2014	BIRA	SAOZ
OHP	France	44°N, 6°E	2011	CNRS	Mini-SAOZ
OHP	France	44°N, 6°E	1992	CNRS	SAOZ
Tarawa	Kiribati Is.	1°N, 173°E	1992/1999	CNRS/NIWA	SAOZ
Seychelles	Seychelles Is.	5°S, 55°E	2017	CNRS	Mini-SAOZ
Reunion	Reunion Is.	21°S, 55°E	1994	CNRS/U. Reunion	SAOZ
Reunion	Reunion Is.	21°S, 55°E	1994	CNRS/U. Reunion	Mini-SAOZ
Bauru	Brazil	22°S, 49°W	1995	CNRS/UNESP	SAOZ
Broadmeadows	Australia	38°S, 145°E	2019	BORN (Meteo)	Mini-SAOZ
Kerguelen	Kerguelen Is.	45°S, 70°E	1995	CNRS	SAOZ
Rio Gallegos	Argentina	52°S, 69°W	2008	CNRS/CITEFA	SAOZ
Faraday	Antarctica	65°S, 64°W	1990/1995	BAS	SAOZ
Zhongstan	Antarctica	69°S, 76° E	2016	China	Mini-SAOZ
Dumont d'Urville	Antarctica	67°S, 140°E	1988	CNRS	SAOZ
Rothera	Antarctica	68°S, 68°W	1996	BAS	SAOZ
Concordia	Antarctica	75°S, 123°E	2007	CNRS	SAOZ
Halley Bay	Antarctica	76°S, 26°W	2013	BAS	SAOZ

2-2 UV-Visible spectroscopic observations

The SAOZ and Mini-SAOZ instruments are looking at the sunlight scattered at zenith. By observing at twilight (solar zenith angles - SZA close to 90°) the solar rays traverse long paths in the atmosphere, typically 300 km, before being scattered by air molecules into the spectrometer's zenith view. At 500 nm, rays below ~12 km tangent point are strongly attenuated by Rayleigh scattering along the slant path. This is because Rayleigh scattering by air molecules is proportional to density.

It is also proportional to (wavelength)$^{-4}$, so that at 400 nm the scattering height is about 22 km at 90°. The fact that the mean scattering height is in the upper troposphere or higher

means that twilight measurements are more sensitive to stratospheric constituents compared to tropospheric ones and thus the zenith sky spectrometers have a high sensitivity to detect stratospheric minor constituents like ozone and NO_2. Figure 3 shows the geometry of observation for different SZA.

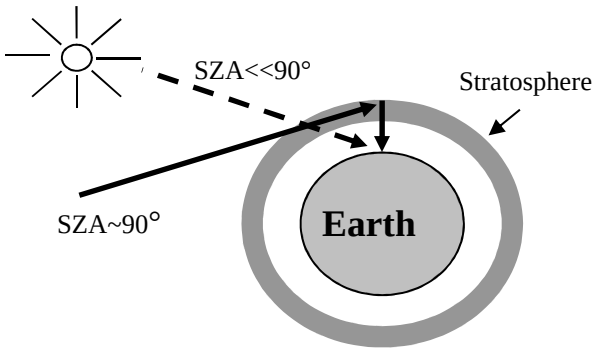

Fig. 3 Path length of solar rays crossing the atmosphere entering in the instrument field of view at high (dotted line) and low Sun (full line).

The first case corresponds to high Sun and small SZA when light rays cross obliquely the atmosphere. The measurements are sensitive to both stratospheric and tropospheric molecules. The second one represents low Sun twilight geometry (SZA near 90°) when light rays cross horizontally the stratosphere and vertically the lower atmosphere. In such a configuration stratospheric measurements (86° to 91° SZA) are little sensitive to tropospheric absorbers.

On cloudy days sunlight is scattered in the lower atmosphere several times before entering the spectrometer. The path length in the lower atmosphere is larger than on clear days. The increase of molecular oxygen dimer, O_4, along the path, measured by SAOZ, allows the correction and proper derivation of H_2O and tropospheric NO_2 columns.

3. Data Analysis

The raw data provided by the instruments are spectra. They are stored in "Level 0" binary files (.**efm files**). The data analysis requires two steps.

The first step is the spectral analysis. The retrieval method used is Differential Optical Absorption Spectroscopy (DOAS), (Platt and Stutz, 2008). It correlates differential narrow features of atmospheric species after removal of the broadband signal due to Raman and Rayleigh scattering, with the differential absorption cross-section of the constituents. It provides slant column, that is the number of molecules along the line-of-sight of each constituent, including ozone, NO_2, H_2O, O_4, O_2. Slant columns as well as ancillary data are recorded in "Level 1" text files (.**mrs files**).

The second step of the analysis is the conversion of the slant column into vertical columns, which requires the use of so-called air mass factors (AMFs) adapted to each constituent. The ozone and NO_2 vertical columns are stored in "Level 2" text files.

3-1 Step 1: Spectral Analysis

The first step is the wavelength alignment followed by the ratio between actual spectrum (I) and a reference spectrum (I_o) recorded with the same instrument at high Sun and clear conditions.

The solar radiation attenuation through the atmosphere is given by the Beer-Lambert law:

$$I = I_0 e^{-\tau} \quad (1)$$

where I_0 and I are radiation before and after crossing the atmosphere and τ is the optical thickness of the atmosphere represented as follows:

$$\tau = \sum \sigma_i(\lambda) * NL_i + \varepsilon_R(\lambda) + \varepsilon_M(\lambda) \quad (2)$$

where the first right term σ_i is the absorption cross-section of the constituent, NL_i its slant column and the second and third terms are Rayleigh and Mie scattering, The right terms depend on wavelength (λ).

The optical absorption spectroscopy equation can be written as:

$$\tau = \ln \frac{I_0(\lambda)}{I(\lambda)} = \sum \sigma_i(\lambda) * NL_i + \varepsilon(\lambda) \quad (3)$$

In the case of SAOZ, the optical thickness is equal to the logarithm of the ratio between actual spectra (I) and the reference spectrum (I_0) recorded at high Sun (ex. at 40° SZA) on a clear and unpolluted day.

The wavelength dependence and the resolution of the reference spectrum are determined accurately. The correspondence between detector pixels and wavelength is determined by looking at the deep and narrow Fraunhofer lines in the reference spectrum. The comparison is made after degrading the high-resolution (0.005nm) solar spectrum (Kurucz et al., 1984) to match the SAOZ reference spectrum resolution.

The wavelength calibration makes use of fifteen Fraunhofer absorption lines to which a parabolic fitting process is applied to shift and stretch the spectrum by least-square correlation between measured and reference spectra. Figure 4. shows the signal and reference spectra and the fifteen Fraunhofer lines used for wavelength fitting.

After wavelength alignment, the DOAS technique, as shown in equation 4, removes the monotonic large variation (2nd and 3rd right terms of eq. 2 or ε in eq. 3). This is done by subtracting the same spectrum smoothed at broad-band pass filter (40 nm) resulting in an atmospheric differential spectrum, into which narrow features are remaining only.

$$\Delta\tau = \sum \Delta\sigma_i(\lambda) * NL_i \quad (4)$$

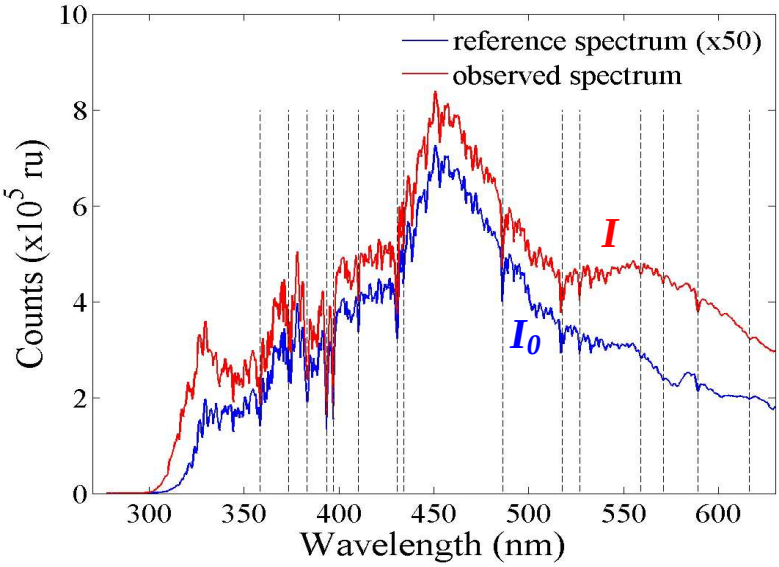

Fig. 4 In red: Spectrum measured at SZA=90° in August 2010. In blue: Reference spectrum at SZA=50° in summer 2002. Dashed lines show the position of Fraunhofer absorption lines.

The resultant differential optical thickness ($\Delta\tau$ in equation 4) contains atmospheric absorption features only. These are identified by fitting laboratory spectra and differential absorption cross-sections $\Delta\sigma_i$ of the various molecules, available in the scientific literature. The cross sections can be updated when new laboratory data become available. So far, spectra of the following constituents are used: NO_2, O_3, O_4, H_2O and O_2.

Slant columns of each constituent (NL_i in equation 4) are then calculated by the least squares fitting between the differential signal $\Delta\tau_i$ and the differential laboratory cross-sections $\Delta\sigma_i$ of each absorber in an iterative process in which the contributions of the various species are calculated and removed sequentially. The width of the filters and the spectral analysis window are adapted to the characteristics of each absorber to reduce interference and enhance absorber features. The differential method allows a self-calibration of constituents on the absorption cross-sections.

Ring effect linked to wavelength redistribution of photons by Raman scattering (Solomon et al., 1997) has to be considered in the iteration steps since it perturbs and deforms the shape of the Fraunhofer lines. A high-resolution Ring effect signature or "cross-section" is generated following Chance and Spurr (1997). This "cross-section" is convolved to the instrumental resolution.

High-resolution absorption cross-sections convolved with the instrument slit function are used to build the cross-section data aligned with the wavelength calibrated reference spectrum. Ozone is measured in the Chappuis visible bands (450-550nm) where the cross sections are not dependent of temperature; NO_2 in 410-530nm range; O_4 in two large bands around 470nm and 570nm; H_2O in two bands around 505nm and 590nm and O_2 around 620nm. Cross-sections settings recommended by NDACC UV-Vis Working Group, especially for ozone retrieval are shown in Table 2.

Table 2 Settings recommended for retrieval of O_3 vertical columns (adapted from Hendrick et al., 2011)

Parameter	Recommendation
Fitting interval for O_3	450-550 nm
Wavelength calibration	based on reference spectrum
Cross sections O_3 NO_2 H_2O O_4 Ring effect	 Bogumil et al., 2003 at 223°K Vandaele et al. 1997, at 220°K Rothman et al., 2005 - Hitran 2004 Hermans (http://spectrolab.aeronomie.be/o2.htm) Ring effect correction from Chance and Spurr (1997)
AMF calculation for O_3	BIRA-IASB O_3 AMF LUTs http://uv-vis.aeronomie.be/groundbased/
Residual amount in reference spectrum	Monthly Langley plot Vaughan et al. 1997
SZA range	86°-91°SZA

Figure 5 shows differential optical thickness of ozone resulting from the first and last iteration steps of spectral analysis. This figure highlights the improvement between step 1 (in black) and the step 5 (in blue), since features of $\Delta\tau_{O3}$ in the last step are showing better correlation with the ones of $\Delta\sigma_{O3}\ NL_{O3}$ represented by red dashed line.

The slope coefficient of the correlation between differential optical thickness and differential absorption cross-section (cf. Figure 5.) gives the ozone slant column amount of NL_{O3}. The standard deviation of the correlation represents the 1σ uncertainty of the measurement.

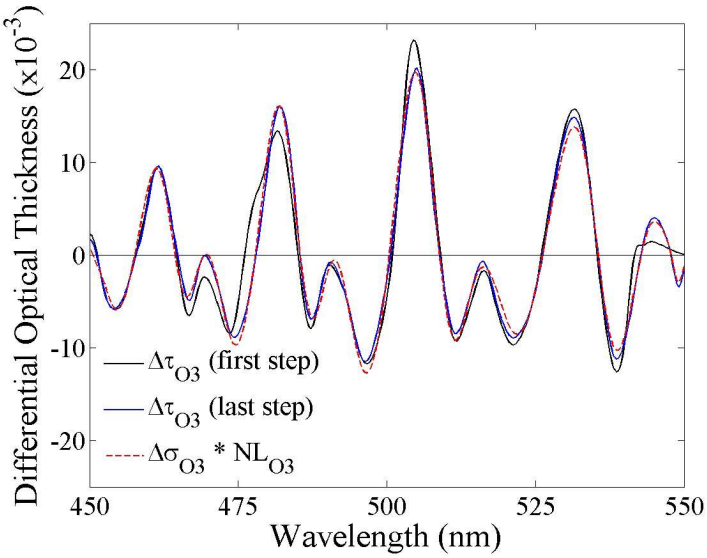

Fig. 5 Ozone spectral analysis: ozone differential optical thickness for the first (in black) and fifth (in blue) iteration. Differential ozone absorption cross sections multiplied by slant column are shown by red dashed line.

Slant column of each constituent NL_i is expressed as follows:

$$NL_i = \frac{\Delta\tau_i}{\Delta\sigma_i} \qquad (5)$$

Figure 6 displays $\Delta\tau_i$ and $\Delta\sigma_i$ multiplied by NL_i where i is for NO_2, O_4 and H_2O after the last step of the spectral analysis (top panels). Differential optical thickness of each constituent presents a good correlation with the corresponding differential absorption cross-section, interferences of others known absorbers in the spectral range after five iterations are negligible. Panel d) of Figure 6, shows the polynomial fitting used for spectral calibration. This fitting presents a small shift and stretch of spectrum with a maximum difference between short and long wavelengths lower than 0.12 pixel (0.04nm in the case shown here).

The spectral displacement due to spectrometer temperature changes are limited and taken into account in the spectral alignment procedure. Panels e) and f) in Figure 6 show the absolute and differential optical thickness before (in blue) and after (in red) spectral analysis. All constituents' signatures are correctly removed from the signal after analysis. The absolute optical thickness in panel e) shows Rayleigh and Mie typical contributions without different features of ozone and others absorbers. The residual differential optical thickness after removal of constituents signatures is smaller than 3/1000 as shown by the blue line in panel f) of Figure 6.

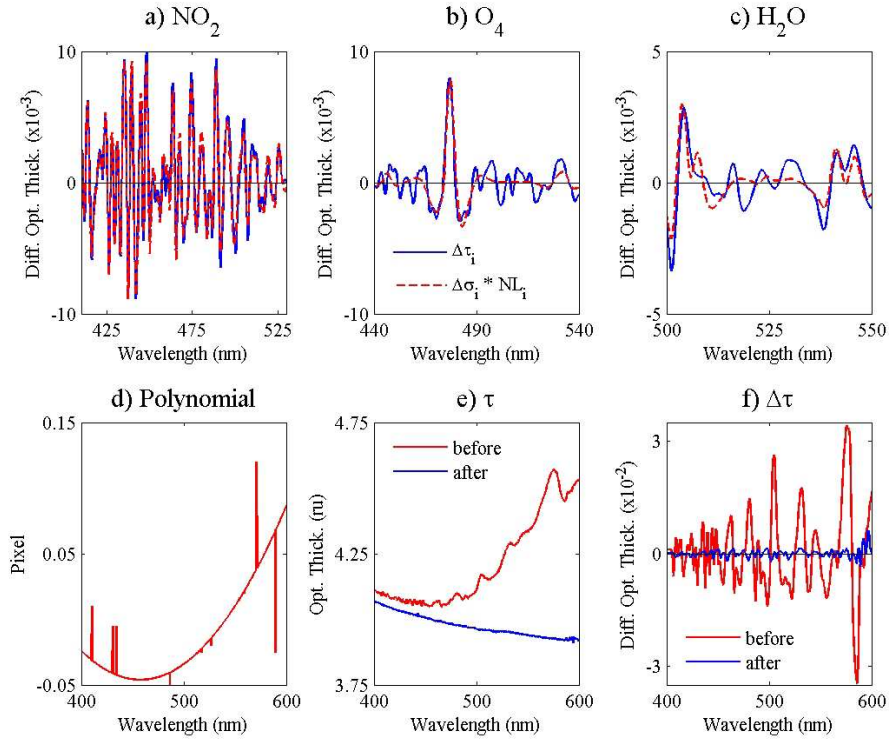

Fig. 6 Top panels: Differential optical thickness and differential absorption cross-section multiplied by calculated slant column of a) NO_2, b) O_4 and c) H_2O after spectral analysis. Bottom panels: d) polynomial curve used for wavelength fitting, e) signal before and after correction of all constituents and f) differential optical thickness before and after spectral analysis.

3-2 Step 2: Ozone and NO2 vertical columns

The conversion of slant columns relative to a given reference spectrum into vertical columns requires the knowledge of the optical path of light scattered at zenith, that is the AMF (Air Mass Factor) and the constituent residual amount in the reference spectrum. Equation 6. shows the calculation of the ozone vertical column (N_{03}):

$$N_{O_3} = \frac{NL_{O_3} + NL_{refO_3}}{AMF_{O_3}} \qquad (6)$$

where NL_{ref03} is the ozone residual amount in the reference spectrum and AMF_{03} the ozone AMF.

3.2.1 Air Mass Factor (AMF)

The length of the light path (the slant path) varies with the SZA. The ratio between slant and vertical columns depends upon the vertical distribution of the constituent (concentration and peak altitude), aerosols, density profiles and wavelength. This ratio (enhancement factor or air-mass factor AMF) is provided by a radiative transfer model in single scattering. Although the AMFs are strongly dependent on multiple scattering (clouds, rain, snow shower and fog) in the lower layers of the atmosphere, the single scattering approximation applies well around 500 nm, where the average scattering layer at 90° SZA is at around 10-12 km below the ozone and nitrogen dioxide peak altitude concentrations and well above tropospheric clouds.

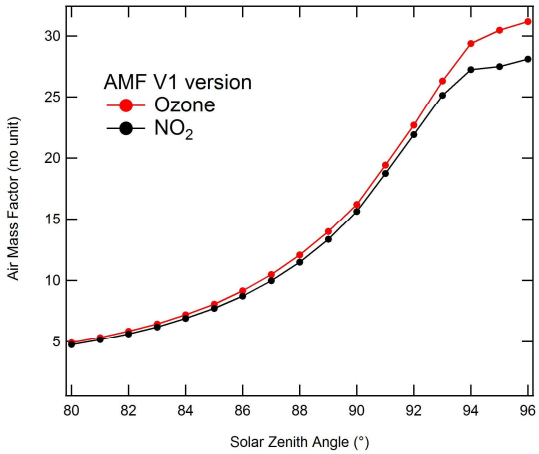

Fig. 7 Ozone and NO_2 Air Mass Factor used in version 1 of SAOZ data.

Until recently (before 2011 for O_3 and before 2013 for NO_2), a single latitude dependent AMF (SAOZ AMF) was used, one for O_3 and one for NO_2. These AMFs were based on mean profiles for the Tropics, Mid-latitudes or Polar regions. The AMF is calculated using a simple radiative transfer model in single scattering approximation at the central wavelength of the fitting band: at 510 nm for O_3 and 470 nm for NO_2 (Sarkissian et al, 1995). For example, at

90° SZA the Polar "SAOZ" AMF was respectively 16.6 for O_3 and 16.1 for NO_2. The vertical columns of O_3 and NO_2 using "SAOZ" AMF is called SAOZ V1 version.

Daily Ozone AMF

In 2010, a daily AMF for ozone calculated by UVSPEC/DISORT radiative transfer model (Mayer et Kylling, 2005) has been implemented in SAOZ V2 re-analysis process. The model uses a multi-entry database from TOMS version 8 (TV8) ozone and temperature profiles climatology (Mc Peters et al., 2007). The TV8 is a monthly-zonal climatology sorted according to the ozone column. The considered parameters are fitting window central wavelength (510nm), station ground albedo and location (latitude, longitude, altitude), day of year, ozone slant column and SZA. The software is available on the Belgian Institute for Space Aeronomie (BIRA-IASB) web site (http://uv-vis.aeronomie.be/groundbased/) as indicated in Table 2.

The impact of using the new daily O_3 AMF (SAOZ V2 algorithm) is described in Hendrick et al., 2011. Figure 8 shows the yearly evolution of daily AMF at 90°SZA and the single AMF used in former SAOZ V1 retrieval for tropical, mid- and high-latitude stations.

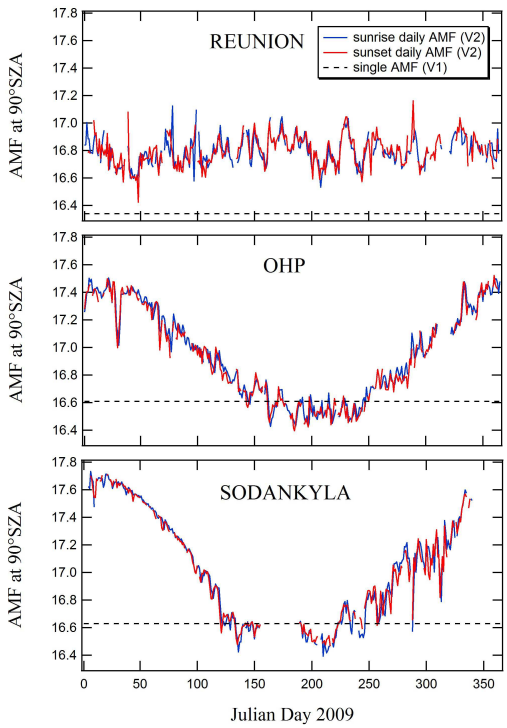

Fig. 8 Seasonal variation of daily (sunrise in red, sunset in blue) and single O_3 AMFs at 90°SZA in 2009 at La Reunion (21°S, 55°E), Observatoire de Haute Provence (OHP) (44°S, 6°E) and Sodankyla, Finland (67°N, 27°E). The SAOZ tropical, mid- and high-latitude O_3 AMFs fixed at 90°SZA are 16.3, 16.6 and 16.6, respectively (dash lines).

In the case of Sodankyla in Finland and Observatoire de Haute Provence (OHP), in France, two stations at high and mid-latitude respectively, the largest difference is obtained in

winter with daily AMFs larger than those of SAOZ by up to 6%. In summer, the difference is in the 0-1% range, with daily AMFs generally lower than SAOZ V1. In the tropics (La Reunion), daily AMFs are systematically larger than SAOZ AMF V1 by up to 4%, with no seasonal variation.

Daily NO_2 AMF

In 2013, a similar work has been performed for NO_2. Daily AMFs calculated by UVSPEC/DISORT radiative transfer model have been introduced in SAOZ V3 re-analysis process. The model uses a multi-entry database from NO_2 sunrise and sunset profiles climatology based on Satellite/SAOZ-balloon data and temperature profiles. The considered parameters are fitting window central wavelength (470nm), station ground albedo and location (latitude, longitude, altitude), day of year, time and SZA. The time of measurement is the important information since NO2 displays a large diurnal variation. The software is available on the Belgian Institute for Space Aeronomie (BIRA-IASB) web site http://uv-vis.aeronomie.be/groundbased/.

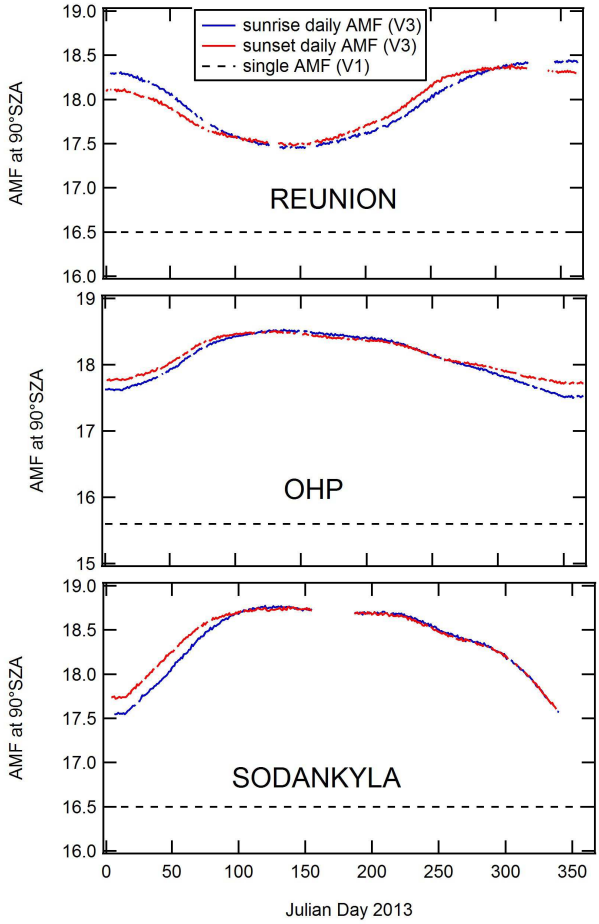

Fig. 9 Seasonal variation of daily (sunrise in red, sunset in blue) and single NO_2 AMFs at 90°SZA in 2013 at La Reunion (21°S, 55°E), Observatoire de Haute Provence (OHP), (44°S, 6°E) and Sodankyla, (67°N, 27°E). The SAOZ tropical, mid- and high-latitude NO_2 AMF fixed at 90°SZA are 16.5, 15.6 and 16.5, respectively (dashed lines).

The impact of using daily NO_2 AMF (SAOZ V3 algorithm) is not published yet. Figure 9 shows preliminary results of the yearly evolution of daily AMFs at 90°SZA and single AMF used in the former SAOZ V1 retrieval for tropical, mid- and high-latitude stations.

The NO_2 daily AMFs are systematically larger than the single SAOZ AMF V1. The difference is larger in summer. In the tropics (Reunion), daily AMFs are larger by 12% in summer and 6% in winter. At mid-latitudes (Observatoire de Haute Provence (OHP), daily AMFs are larger by 18% in summer and 13% in winter. At high-latitudes (Sodankyla) the difference is 13% in summer and 7% in winter.

3.2.2 Residual

In order to minimize the number density of the constituent along the line of sight, the reference spectrum is recorded at high Sun elevation. However, there is still a residual amount of ozone and NO_2 in the reference spectrum. This residual is determined by monthly Bouguer-Langley plot (slant column versus AMF) extrapolated to zero air mass (Vaughan et al., 1997). Another way to show Bouguer-Langley plots is to display vertical column of constituent versus AMF. Figure 10. shows Ozone Bouguer-Langley plots for January and July 2009 at OHP. In this example, the residual O_3 amount in the reference spectrum is $8x10^{18}$ mol./cm^2. This value is correct since the Bouguer-Langley plots are mostly flat for different months as shown in Figure 10. If the residual value was overestimated (underestimated), the curves would present negative (positive) slopes.

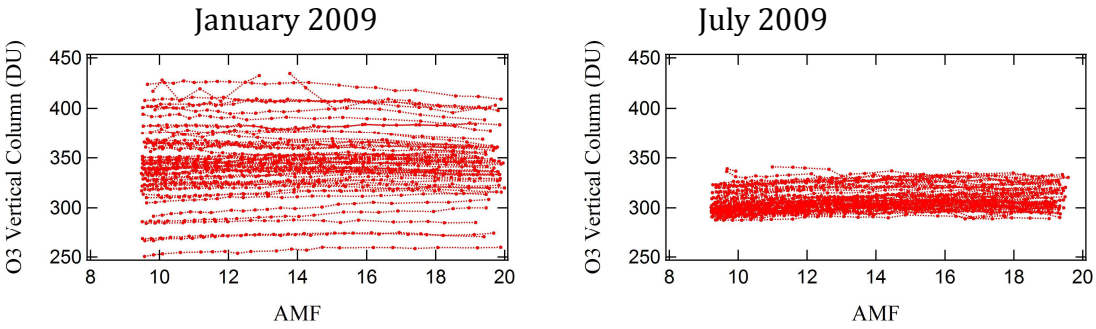

Fig. 10 Ozone Column Bouguer-Langley plots corresponding to an ozone residual amount of $8x10^{18}$ mol./cm^2 (297 DU) in the reference spectrum at OHP.

3.2.3 Error budget

The overall error budget on V2 O_3 vertical columns takes into account uncertainties on cross-sections, AMF (constituent vertical profiles, stratospheric temperature seasonal variation) and the residual amount in the reference spectrum. The total error for O_3 is estimated to 4.6 % (Hendrick et al., 2011).

The overall error budget on V3 NO_2 vertical columns takes into account uncertainties on cross-sections, AMF (sunrise and sunset profiles, stratospheric temperature seasonal cycle),

NO_2 photochemical variation during daytime and residual amount in reference spectrum. A preliminary error budget for NO_2 of 10-15% is estimated.

3-3 Clouds detection

The presence of clouds can be identified by looking at a colour index, the most sensitive one being the ratio between two fluxes in 550nm and 350nm. In addition their altitude can be derived from the SZA at which the maximum reddening occurs.

Very large colour indices can be observed sometimes at twilight in winter due to the presence of high altitude Polar Stratospheric Clouds (PSCs), (Sarkissian et al., 1991).

Measured spectra, calculated columns and colour index (CI) are recorded on the PC computer and available on the SAOZ web site: http://saoz.obs.uvsq.fr/SAOZ-RT.html .

3-4 Bibliography

Bogumil, K., Orphal, J., Homann, T., et al.: Measurements of molecular absorption spectra with the SCIAMACHY Pre-Flight Model: Instrument characterization and reference spectra for atmospheric remote sensing in the 230-2380 nm region, J. Photochem. Photobiol. A, 157, 167-184, 2003.

Chance, K. and Spurr, R. J. D.: Ring effect studies: Rayleigh scattering including molecular parameters for rotational Raman scattering, and the Fraunhofer spectrum, Applied Optics, 36, 5224-5230, 1997.

Hendrick, F., J.-P. Pommereau, F. Goutail, et al., NDACC/SAOZ UV-visible total ozone measurements: improved retrieval and comparison with correlative ground-based and satellite observations, Atmos. Chem. Phys., 11(12), 5975-5995, 2011, doi:10.5194/acp-11-5975-2011.

Kurucz, R. L., Furenlid, I., and Brault, J. T. L.: Solar flux atlas from 296 to 1300 nm, National Solar Observatory Atlas, Sunspot, New Mexico, 1984.

McPeters, R. D., Labow, G. J., and Logan, J. A.: Ozone climatological profiles for satellite retrieval algorithms, J. Geophys. Res., 112, D05308, doi:10.1029/2005JD006823, 2007.

Mayer, B. and Kylling, A.: Technical note: The LibRadtran software package for radiative transfer calculations – Description and examples of use, Atmos. Chem. Phys., 5, 1855–1877, 2005.

Platt, U. and Stuz, J.: Differential Optical Absorption Spectroscopy (DOAS), Principles and Applications, ISBN 978-3-540-21193-8, Springer, Berlin-Heidelberg, 2008.

Pommereau, J.P. and F. Goutail, Stratospheric O3 and NO2 Observations at the Southern Polar Circle in Summer and Fall 1988, Geophys. Res. Lett., 895, 1988.

Rothman, L. S., Jacquemart, D., Barbe, at al.: The Hitran 2004 molecular spectroscopic database, J. Quant. Spectrosc. Ra., 96, 139–204, 2005.

Sarkissian A., J.P. Pommereau and F. Goutail, Identification of Polar Stratospheric Clouds from the ground by visible spectrometry, Geophys. Res. Lett., 18, 779-782, 1991.

Sarkissian, A., Roscoe, H. K., Fish, et al.: Ozone and NO_2 AMF for zenith sky spectrometer: Intercomparison of calculations with different radiative transfer model, Geophys. Res. Lett., 22, 1113-1116, 1995.

Solomon, S., Schmeltekopf, A. L., and Sanders, R. W.: On the interpretation of zenith-sky absorption measurements, J. Geophys. Res., 92, 8311-8319, 1987.

Vandaele, A. C., Hermans, C., Simon, P. C., Carleer, M., Colin, R., Fally, S., Mérienne, M.-F., Jenouvrier, A., and Coquart, B.: Measurements of the NO_2 absorption cross section from 42000 cm^{-1} to 10000 cm^{-1} (238-1000 nm) at 220 K and 294 K, J. Quant. Spectrosc. Radiat. Transfer, 59, 171-184, 1997.

Vaughan G., H. K Roscoe, L.M. Bartlett, F.M. et al., An intercomparison of ground-based UV- visible sensors of Ozone and NO_2, J. Geophys. Res., **102**, 1411-1422, 1997.

3-5 SAOZ/Mini-SAOZ references

More than 120 publications using SAOZ data can be found in peer-review literature. Here below a selection of papers.

Goutail, F., J-P. Pommereau, C. Phillips, C. Deniel, A. Sarkissian, F. Lefevre, E. Kyro, M. Rummukainen, P. Ericksen, S.B. Andersen, B-A Kaastadt Hoiskar, G. Braathen, V. Dorokhov and V.U. Khattatov, Depletion of column ozone in the Arctic during the winters of 1993-94 and 1994-95, J. Atm. Chem., 32, 1-34, 1999.

Goutail, F., J.-P. Pommereau, F. Lefèvre, M. Van Roozendael, S. B. Andersen, B.-A. Kåstad Høiskar, V. Dorokhov, E. Kyro, M. P. Chipperfield and W. Feng, Early unusual ozone loss during the Arctic winter 2002/03 compared to other winters, Atmos. Chem. Phys., ACP-2004-SI01004, 2005.

Piters, A. J. et al..: The Cabauw Intercomparison campaign for Nitrogen Dioxide measuring Instruments (CINDI): design, execution, and early results, Atmos. Meas. Tech., 5(2), 457-485, https://doi.org/10.5194/amt-5-457-2012, 2012.

Pommereau, J.-P., Goutail, F., Lefèvre, F., Pazmino, A., et al..: Why unprecedented ozone loss in the Arctic in 2011? Is it related to climate change?, Atmos. Chem. Phys., 13 (10), 5299-5308, https://doi.org/10.5194/acp-13-5299-2013, 2013.

Dieudonné, E., F. Ravetta, J. Pelon, F. Goutail, and J.-P. Pommereau, Linking NO_2 surface concentration and integrated content in the urban developed atmospheric boundary layer, Geophys. Res. Lett., 40, 1247–1251, https://doi.org/10.1002/grl.50242, 2013.

Koukouli, M., D. Balis, E. Zyrichidou, et al., Validating the new GOME/ERS-2, SCIAMACHY/Envisat and GOME-2/MetOp-A homogeneous total ozone climate data record developed as part of the ESA Climate Change Initiative, J. Geophys. Res. Atmos., American Geophysical Union, 2015, 120 (23), 12296-12312, https://doi.org/10.1002/2015JD023699, 2015.

Verhoelst, T., J. Granville, et al., Metrology of ground-based satellite validation: co-location mismatch and smoothing issues of total ozone comparisons, Atmos. Meas. Tech., 8, 5039-5062, https://doi.org/10.5194/amt-8-5039-2015, 2015.

Tack, F., F. Hendrick, F. Goutail, et al., Tropospheric nitrogen dioxide column retrieval from ground-based zenith-sky DOAS observations, Atmos. Meas. Tech., 8, 2417-2435, https://doi.org/10.5194/amt-8-2417-2015, 2015.

Boynard, A., D. Hurtmans, M. E. Koukouli, F. Goutail, et al., Seven years of IASI ozone retrievals from FORLI: validation with independent total column and vertical profile measurements, Atmos. Meas. Tech., European Geosciences Union, 9 (9), 4327-4353, https://doi.org/10.5194/amt-9-4327-2016, 2016.

Garane K., Lerot C., Coldewey-Egbers M., at al., Quality assessment of the Ozone_cci Climate Research Data Package (release 2017) – Part 1: Ground-based validation of total ozone column data products, Atmos. Meas. Tech., 11, 1385-1402, https://doi.org/10.5194/amt-11-1385-2018, 2018.

Bognar K., X. Zhao et al., Validation of ACE and OSIRIS ozone and NO2 measurements in the Arctic using ground-based instruments at Eureka, Canada, Journal of Quantitative Spectroscopy and Radiative Transfer, Elsevier, 238 (November), pp.art. 106571. https://doi.org/10.1016/j.jqsrt.2019.07.014, 2019.

Garane K., Koukouli M.-E., et al., TROPOMI/S5ptotal ozone column data: global ground-based validation & consistency with other satellite missions, Atmos. Meas. Tech., European Geosciences Union, 12 (10), 5263-5287, https://doi.org/10.5194/amt-12-5263-2019, 2019.

Compernolle S., Verhoelst T., et al., Validation of Aura-OMI QA4ECV NO2 Climate Data Records with ground-based DOAS networks: role of measurement and comparison uncertainties, Atmos. Chem. Phys., European Geosciences Union, 8017–8045, https://doi.org/10.5194/acp-20-8017-2020, 2020.

Kreher, K. et al., Intercomparison of NO2, O4, O3 and HCHO slant column measurements by MAX-DOAS and zenith-sky UV-visible spectrometers during CINDI-2, Atmos. Meas. Tech., European Geosciences Union, 13 (5), 2169-2208, , https://doi.org/10.5194/amt-13-2169-2020, 2020.

Verhoelst, T., S. Compernolle, et al. Ground-based validation of the Copernicus Sentinel-5p TROPOMI NO2measurements with the NDACC ZSL-DOAS, MAX-DOAS and Pandonia global networks, Atmos. Meas. Tech. Discuss., (Accepted in ACP), https://doi.org/10.5194/amt-2020-119, 2020.